

Discovery of a transient ultraluminous X-ray source in the elliptical galaxy M86

Lennart M. van Haaften,^{1*} Thomas J. Maccarone,¹ Katherine L. Rhode,²
Arunav Kundu,^{1,3,4} and Stephen E. Zepf⁵

¹*Department of Physics and Astronomy, Texas Tech University, Box 41051, Lubbock, TX 79409-1051, USA*

²*Department of Astronomy, Indiana University, 727 East Third Street, Bloomington IN 47405, USA*

³*Eureka Scientific, Inc., 2452 Delmer Street, Suite 100, Oakland, CA 94602, USA*

⁴*Computational Physics, Inc., 8001 Braddock Road, Suite 210, Springfield, VA 22151, USA*

⁵*Department of Physics and Astronomy, Michigan State University, East Lansing, MI 48824, USA*

Accepted 2018 November 23. Received 2018 November 20; in original form 2018 July 20

ABSTRACT

We report the discovery of the transient ultraluminous X-ray source (ULX) CXOU J122602.3+125951 (hereafter M86 tULX-1), located 3'52" (19 kpc) northwest of the centre of the giant elliptical galaxy M86 (NGC 4406) in the Virgo Cluster. The spectrum of M86 tULX-1 can be fit by a power-law plus multicolour-disc model with a $1.0^{+0.8}_{-2.6}$ index and an $0.66^{+0.17}_{-0.11}$ keV inner-disc temperature, or by a power law with a 1.86 ± 0.10 index. For an isotropically emitting source at the distance of M86, the luminosity based on the superposition of spectral models is $(5 \pm 1) \times 10^{39}$ erg s⁻¹. Its relatively hard spectrum places M86 tULX-1 in a hitherto unpopulated region in the luminosity-disc temperature diagram, between other ULXs and the (sub-Eddington) black-hole X-ray binaries. We discovered M86 tULX-1 in an archival 148-ks 2013 July *Chandra* observation, and it was not detected in a 20-ks 2016 May *Chandra* observation, meaning it faded by a factor of at least 30 in three years. Based on our analysis of deep optical imaging of M86, it is probably not located in a globular cluster. It is the brightest ULX found in an old field environment unaffected by recent galaxy interaction. We conclude that M86 tULX-1 may be a stellar-mass black hole of $\sim 30 - 100 M_{\odot}$ with a low-mass giant companion, or a transitional object in a state between the normal stellar-mass black holes and the ultraluminous state.

Key words: X-rays: individual: CXOU J122602.3+125951 – X-rays: binaries – stars: black holes – galaxies: individual: M86, NGC 4406

1 INTRODUCTION

Ultraluminous X-ray sources (ULXs) are point-like X-ray sources brighter than the 2×10^{39} erg s⁻¹ Eddington luminosity of stellar-mass ($M \lesssim 20 M_{\odot}$, Begelman 2002; Zezas & Fabiano 2002) black holes (BHs) that are not located in galactic centres (for recent reviews, see Bachetti 2016; Kaaret et al. 2017). Most ULXs are thought to be either stellar-mass BHs, or BHs with masses in the range of 30 – 90 M_{\odot} (Zampieri & Roberts 2009), or neutron stars (NSs) (Bachetti et al. 2014; Fürst et al. 2016; Israel et al. 2017b,a) accreting above their Eddington limits, possibly in some cases with beamed emission (King et al. 2001; Poutanen et al. 2007). One of the arguments in favour of super-Eddington accretion is that many ULX spectra show a soft excess in combination with a hard component with a high-energy curvature

above ~ 3 keV, which has been interpreted as an optically thick radiatively driven wind from the outer accretion disc, pointing to an ultraluminous (UL) state (Roberts 2007; Soria 2007; Gladstone et al. 2009; Sutton et al. 2013). The wind scenario is also supported by the detection of blueshifted absorption lines in the high-resolution X-ray spectra of several ULXs (Pinto et al. 2016; Kosec et al. 2018). Especially ULXs with X-ray luminosity $L_X = (3 - 20) \times 10^{39}$ erg s⁻¹ have spectra consistent with stellar-mass BHs in the UL state (Middleton et al. 2015). Alternatively, intermediate-mass black holes (IMBHs) with masses of $\sim 10^2 - 5 M_{\odot}$ could produce the observed X-ray luminosities with sub-Eddington accretion rates (Colbert & Mushotzky 1999), and are plausible explanations for at least the ULXs with $L_X \gtrsim 5 \times 10^{40}$ erg s⁻¹ (Farrell et al. 2009; Davis et al. 2011; Webb et al. 2012).

Clear differences exist between the properties of ULXs in different environments. ULXs are most commonly found in spiral galaxies (Swartz et al. 2004), starburst galaxies

* E-mail: L.vanHaaften@ttu.edu

(e.g., Fabbiano et al. 2001; Lira et al. 2002), and in or close to star-forming regions within galaxies (Swartz et al. 2009). The association with star-forming regions favours highly magnetic NS accretors (Shao & Li 2015; King & Lasota 2016; Pintore et al. 2017; Koliopanos et al. 2017) and/or high-mass donor stars (Swartz et al. 2009; Liu 2009; Motch et al. 2011; Poutanen et al. 2013), although it is difficult to distinguish optical emission from a companion star from accretion disc emission (e.g., Copperwheat et al. 2005, 2007; Patruno & Zampieri 2008; Madhusudhan et al. 2008).

Smaller numbers of ULXs are located in elliptical galaxies. In particular bright ULXs, with $L_X \gtrsim 2 \times 10^{39}$ erg s $^{-1}$, are extremely rare in elliptical galaxies (Irwin et al. 2004; Peacock & Zepf 2016), although some are known in globular clusters in ellipticals (Maccarone et al. 2007; Irwin et al. 2010). This suggests that bright ULXs in old populations typically have different origins and properties than equally bright ULXs in young environments, and also different from less bright ULXs in old environments, perhaps by means of having a more massive BH accretor.

In this paper we report the discovery of CXOU J122602.3+125951 (hereafter M86 tULX-1), a ULX, in the giant Virgo Cluster elliptical galaxy M86. In Sect. 3, we report on this source’s X-ray variability, spectrum, and luminosity, and our search for counterparts in archival optical data. In Sect. 4, we compare this source’s properties and environment to those of other bright ULXs. We also discuss possible accretor type and mass, and the companion star. Finally, in Sect. 4.4, we argue that M86 tULX-1 is genuinely located in M86, and not a foreground or background object.

2 OBSERVATIONS AND DATA ANALYSIS

We used a 148-ks archival *Chandra* Advanced CCD Imaging Spectrometer I (ACIS-I) observation from 2013 July, ObsID 15149, with PI Scott Randall. In 2016 May, prior to M86 tULX-1’s discovery, we obtained a 20-ks ACIS-I observation, ObsID 16967, aimed at the centre of M86. More details of these observations are listed in Table 1. We identified sources in these two observations with the CIAO tool WAVDETECT (Freeman et al. 2002), with the SIGTHRESH parameter set at 10^{-6} , and the SCALES values a geometric progression with a constant factor of $\sqrt{2}$ between 2 and 16.

We extracted and modeled the *Chandra* spectrum and (upper limit to the) flux of M86 tULX-1 using the CIAO software package. We used a circular source region around M86 tULX-1 with radius of $4''.6$ and an annular background region with inner and outer radii of $4''.6$ and $23''.2$, respectively. Neutral hydrogen in the interstellar medium absorbs part of the soft X-rays, which the spectral models take into account. The Galactic column density of neutral hydrogen atoms has an average value of $N_H \approx 2.62 \times 10^{20}$ cm $^{-2}$ in the direction of M86, according to the HEASARC W3 N_H tool. In order to avoid degeneracy between the spectral parameters, we froze the N_H parameter at this value in the spectral fits.

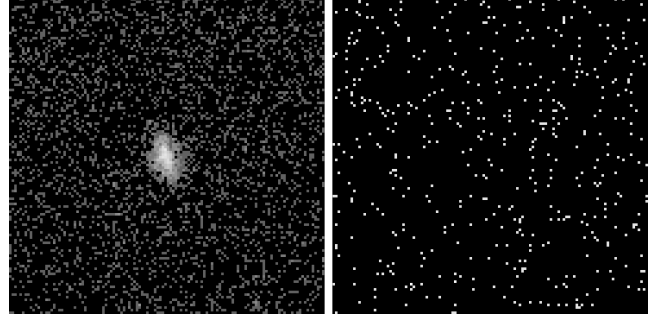


Figure 1. *Chandra* images of the 1×1 arcmin field centred around M86 tULX-1 on 2013 July 24-25 (left), and the same field on 2016 May 2 (right).

3 RESULTS

3.1 Source location

M86 is a member of the Virgo Cluster. The centre of the galaxy is located at R.A. $12^{\text{h}} 26^{\text{m}} 11^{\text{s}}.814$, Dec $+12^{\circ} 56' 45''.49$ (Skrutskie et al. 2006). We adopted a distance to M86 of 16.83 ± 0.54 Mpc (Mei et al. 2007) to convert flux rates to luminosities.

We found M86 tULX-1 at R.A. $12^{\text{h}} 26^{\text{m}} 02^{\text{s}}.30$, Dec $+12^{\circ} 59' 51''.1$ (J2000 coordinates) in ObsID 15149. The projected distance of M86 tULX-1 to the centre of M86 is $3''.86$, which at the distance of the galaxy is equivalent to 19.3 kpc. Since the effective radius of M86 is $3''.38 \pm 0''.24$ (Kormendy et al. 2009), the galactocentric radius of M86 tULX-1 corresponds to 1.14 effective radii.

The off-axis angle of M86 tULX-1 in ObsID 15149 is $6''.11$, and in ObsID 16967, in which this source is not detected, $3''.86$ (the same as the galactocentric distance, since the aimpoint of ObsID 16967 is at the centre of the galaxy).

The field around M86 tULX-1 in the two *Chandra* observations is shown in Fig. 1.

3.2 Light curve during bright epoch

The light curve of M86 tULX-1 during the 41-hour exposure in 2013 July is shown in Fig. 2. The normalised rms deviation is 0.18 for 3000-s bins for the 0.5 – 8 keV energy range. The normalised excess variance (Turner et al. 1999) of the light curve is $(-1 \pm 8) \times 10^{-3}$ for 3000-s bins. This insignificant excess suggests an absence of variability, which is confirmed by the Fourier power spectrum.

3.3 X-ray spectrum and luminosity during bright epoch

In the bright epoch, M86 tULX-1 had a background-subtracted count rate of $(8.64 \pm 0.25) \times 10^{-3}$ counts s $^{-1}$ (1σ confidence interval) in ObsID 15149. The total X-ray photon count is 1.28×10^3 .

We fitted the unbinned spectrum of M86 tULX-1 with an absorbed power-law model (POWLAW1D), with an absorbed multicolour disc blackbody model (DISKBB), and with a superposition of both models. The resulting POWLAW1D power-law indices and DISKBB inner disc temperatures are listed in Table 2. A χ^2 statistic with the Gehrels variance

Table 1. *Chandra* observations of M86 used in this paper.

Observation ID	Instrument	Exposure time (ks)	Data mode	RA	Dec	Start date and time (UTC)
15149	ACIS-I	148.07	Very Faint	12 25 42.13	+13 03 29.33	2013 Jul 24 04:22:25
16967	ACIS-I	19.81	Faint	12 26 11.80	+12 56 45.50	2016 May 2 06:37:07

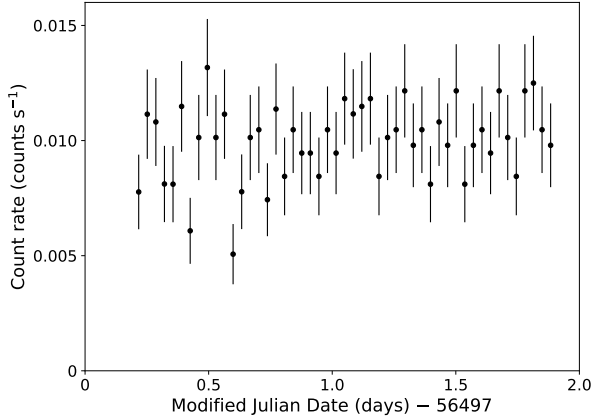

Figure 2. Light curve of M86 tULX-1 during its bright epoch in 2013 July using 3000-second time bins, for the 0.5–8 keV energy range. The average number of counts per bin is 29.5.

Table 2. Spectral fits of M86 tULX-1 for the 0.5–8 keV range. T_{in} is the inner disc temperature. The total flux and DISKBB component flux are in units of $10^{-13} \text{ erg s}^{-1} \text{ cm}^{-2}$, which corresponds to $(3.4 \pm 0.2) \times 10^{39} \text{ erg s}^{-1}$ in M86 (the error is due to the uncertainty in the distance to M86). The XSPEC (Arnaud 1996) goodness of fit of a model is the percentage of simulations based on that model with a test statistic less than that of the data. Confidence limits are 1σ .

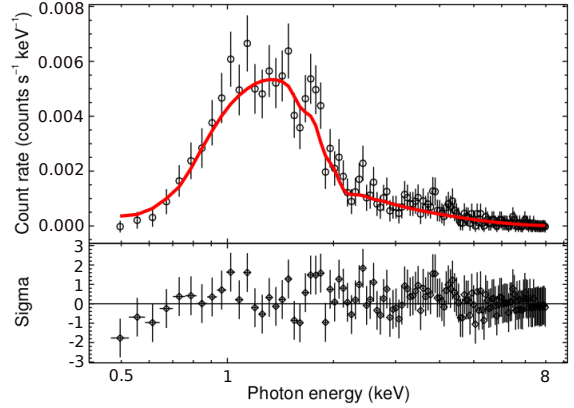
Model	Power-law index	T_{in} (keV)	Flux	DISKBB flux	Goodness
POWLAW1D	1.86 ± 0.10		1.60 ± 0.07		55%
DISKBB		0.87 ± 0.08	0.98 ± 0.04		90%
POWLAW1D+DISKBB	$1.0^{+0.8}_{-2.6}$	$0.66^{+0.17}_{-0.11}$	$1.42^{+0.54}_{-0.18}$	$0.6^{+0.9}_{-0.4}$	59%

function has been used (Gehrels 1986), and the background has been subtracted.

The spectrum of M86 tULX-1 can be best fit (goodness of fit closest to 50 per cent) by a power-law plus multicolour disc model with a $1.0^{+0.8}_{-2.6}$ index and an $0.66^{+0.17}_{-0.11}$ keV inner disc temperature, as shown in Fig. 3, or with an absorbed power-law model with index 1.86 ± 0.10 . The large errors for the superposition model are the consequence of neither component model dominating – a wide range of combinations of two components give a reasonably good fit. For an isotropically emitting source at the distance of M86, the luminosity based on this spectral model is $(5 \pm 1) \times 10^{39} \text{ erg s}^{-1}$, where the error is due to the error in flux rate, as well as due to the error in the distance to M86.

3.4 Upper limit during faint epoch

Using the CIAO tool SRCFLUX, we determined the upper limit to the flux of an undetected source in ObsID 16967


Figure 3. Upper panel: X-ray spectrum of M86 tULX-1 for the 0.5–8 keV range. The red curve shows the power-law plus disc blackbody fit with power-law index of 1.0 and inner disc temperature of 0.66 keV. Bottom panel: Residuals of the fit. Error bars are 1σ .

using the point-spread function area and location of the detection in ObsID 15149, when it was bright. The 3σ limit is $f_X \approx 4.5 \times 10^{-15} \text{ erg s}^{-1} \text{ cm}^{-2}$ for the 0.5–8 keV energy range, about 30 times fainter than M86 tULX-1 during its bright epoch.

We checked archival *XMM-Newton* data to see if M86 tULX-1 has been detected. Using the FLIX tool for *XMM-Newton* upper limits¹ at the location of M86 tULX-1, we found an upper limit of $f_X = (1.3 \pm 0.3) \times 10^{-14} \text{ erg s}^{-1} \text{ cm}^{-2}$ in the 0.5–4.5 keV band for a MOS-2 CCD observation (ID 0108260201) from 2002 July, and an upper limit of $f_X = (3.7 \pm 4.6) \times 10^{-15} \text{ erg s}^{-1} \text{ cm}^{-2}$ for a pn CCD observation (ID 0673310101) from 2011 June, using a detection likelihood threshold of 10, and a $5''$ radius. The source is not significantly detected in these observations, and we did not analyse them further. The *XMM* upper limit for the 2011 June observation is similar to the *Chandra* value from 2016 May, and corresponds to $L_X = (1.3 \pm 1.6) \times 10^{38} \text{ erg s}^{-1}$.

3.5 Archival optical data

We used archival *B*-, *V*-, and *R*-band photometric data that were obtained with the Kitt Peak 4-m telescope and mosaic camera for the purpose of studying the globular cluster population of M86 (Rhode & Zepf 2004; Young 2016). The optical data at the location of M86 tULX-1 were taken on

¹ https://www.ledas.ac.uk/flix/flix_dr7.html

1999 March 24, over 14 years earlier than the two X-ray observations we analysed. The positions of the optical sources have typical 1σ errors of $0''.2$. The positional uncertainty of M86 tULX-1 is $0''.3$. The nearest source to M86 tULX-1 is located at a distance of $13''.3$, so no optical counterpart associated with M86 tULX-1 is detected. Several of the nearby optical sources have been identified based on their magnitudes and colours as globular cluster (GC) candidates; the closest of these is located at $15''.0$ from M86 tULX-1. The 50 per cent detection completeness limit for point sources is $m_V = 24.17$; GCs are usually brighter than this (Forbes et al. 1996). Furthermore, because of the large distribution in GC masses, the percentage of GC stellar mass located in GCs fainter than this limit is significantly lower than the percentage of GCs fainter than this limit themselves. 1.9 per cent of GC mass is located in undetected GCs, based on the luminosity function for M86 in Forbes et al. (1996). Therefore, M86 tULX-1 is probably not located in a GC.

We also note that no sources within 10 arcsec in any wavelength band are listed in Vizier database of astronomical catalogues (Ochsenbein, Bauer & Marcout 2000).

4 DISCUSSION

4.1 Comparison with other ULXs

We highlight some of the unusual properties of M86 tULX-1 and its environment by comparing this source with other ULXs.

4.1.1 Luminosity and environment

The lack of ULXs in elliptical galaxies is consistent with a break near $L_X = 5 \times 10^{38} \text{ erg s}^{-1}$ in the X-ray luminosity function of elliptical galaxies not affected by recent mergers (Sarazin et al. 2000; Kim & Fabbiano 2010). ULXs with $L_X \gtrsim 2 \times 10^{39} \text{ erg s}^{-1}$ are extremely rare in old populations. The catalogue by Swartz et al. (2011) lists two ULXs in the elliptical galaxy NGC 4150 with $L_X \approx (5.6; 10.8) \times 10^{39} \text{ erg s}^{-1}$, but this galaxy has star forming regions near these sources, especially near the brighter of the two. Several bright ULXs have been found in GCs, e.g., in NGC 1399 at $L_X = 5 \times 10^{39} \text{ erg s}^{-1}$ (Angelini et al. 2001; Feng & Kaaret 2006), and a black-hole system in NGC 4472 (Maccarone et al. 2007). Overall, M86 tULX-1 may be the brightest ULX in an old field environment, unaffected by recent dynamical encounters. M86 tULX-1 is the second ULX identified in M86, after CXO J122611.830+125647.80 at $L_X = 2.2 \times 10^{39} \text{ erg s}^{-1}$ (Liu 2011).

4.1.2 Spectral hardness

The inner disc temperature of 0.66 keV is hotter than typical for ULXs, but also cooler than most Galactic black-hole X-ray binaries (Kajava & Poutanen 2009). Combined with its soft excess X-ray luminosity of $L_X = (1.9^{+2.8}_{-1.3}) \times 10^{39} \text{ erg s}^{-1}$, M86 tULX-1 is located in an unpopulated region of the disc temperature-soft excess luminosity diagram (Kajava & Poutanen 2009, their fig. 4), which we reproduced in our

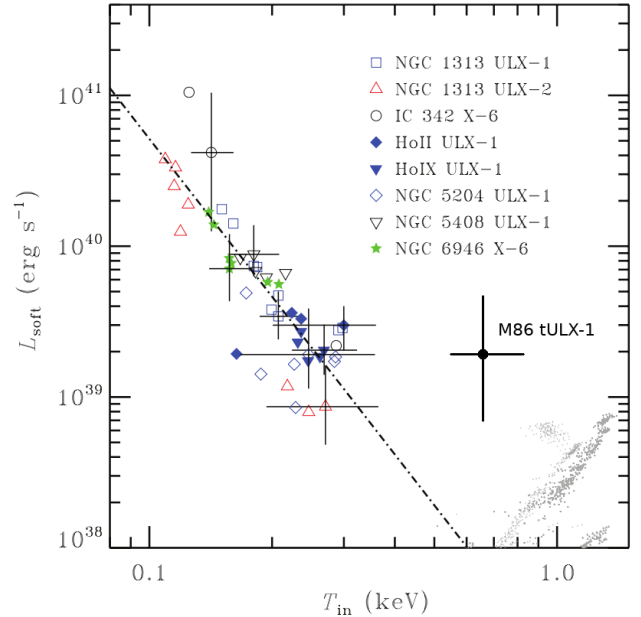


Figure 4. Luminosity-temperature diagram of the soft excess of a sample of ULXs and Galactic X-ray binaries, reproduced with permission from Kajava & Poutanen (2009, their fig. 4). M86 tULX-1 has been added as a black dot.

Fig. 4. The object thus is consistent with being a transitional object, between the bright ULXs and ‘normal’ X-ray binaries.

4.1.3 Variability

ULXs in star-forming environments have been found to be more variable than those in old populations, which are mostly persistent (Feng & Kaaret 2006; Kaaret et al. 2017). For example, CXOU J132518.2–430304, a ULX in Centaurus A, became brighter by a factor of over 770 in four years (Sivakoff et al. 2008). CXOU J235808.7–323403, a ULX in NGC 7793, increased in luminosity from $L_X < 5 \times 10^{37} \text{ erg s}^{-1}$ to $L_X = 3.5 \times 10^{39} \text{ erg s}^{-1}$ (a factor of > 70) in one year (Motch et al. 2014), whereas NGC 5907 ULX-2 became brighter by a factor of over 35 to reach $L_X = 6.4 \times 10^{39} \text{ erg s}^{-1}$ (Pintore et al. 2018). All ULXs hosting NSs have been found to be variable by factors of ~ 200 (Fürst et al. 2016), and over 500 (Israel et al. 2017a; Carpano et al. 2018).

In old populations, several sources show outbursts on top of an already bright baseline. Short-duration flares have been observed up to $\sim 9 \times 10^{40} \text{ erg s}^{-1}$ in a GC source (Irwin et al. 2016). XMMU 122939.7+075333, a $L_X = 4 \times 10^{39} \text{ erg s}^{-1}$ black-hole X-ray binary in a GC, was found to fade to $L_X = 1 \times 10^{38} \text{ erg s}^{-1}$, a factor of 40 (Maccarone et al. 2010; Joseph et al. 2015). CXO J122518.6+144545, either a hyperluminous X-ray source or a field ULX, varied by a factor 60 (Heida, Jonker & Torres 2015). Generally, ULXs in old (field) populations are rarely as variable as M86 tULX-1.

4.2 Accretor type and mass

Based on its high luminosity of $L_X \approx (3 - 6) \times 10^{39} \text{ erg s}^{-1}$ and its variability, M86 tULX-1 likely contains a BH. A $1.4 M_\odot$ NS accretor would imply an accretion rate of 34 times the Eddington limit assuming hydrogen-rich matter, and 17 times in case of helium or carbon/oxygen (assuming only electron scattering contributes to opacity). Four ULXs hosting NSs with higher luminosities than M86 tULX-1 have been discovered (Bachetti et al. 2014; Fürst et al. 2016; Israel et al. 2017b,a; Brightman et al. 2018) as well as one with similar luminosity (Carpano et al. 2018). These may have very strong magnetic fields, allowing X-ray luminosities to be around $10^{40} \text{ erg s}^{-1}$ via accretion (Ekşi et al. 2015; Dall’Osso et al. 2015; Mushtukov et al. 2015; Tsygankov et al. 2016) or spin-down (Medvedev & Poutanen 2013), or alternatively, may have weaker magnetic fields of order 10^{12} G (Walton et al. 2018a,c). High magnetic field neutron stars are short-lived (Thompson & Duncan 1995) and associated with supernova remnants and recent star formation (e.g., Kaspi & Beloborodov 2017). In addition, the masses of companion stars to NS ULXs are observed or inferred to be over $5 M_\odot$ (e.g., Karino 2018). Located in an old environment, M86 tULX-1 is unlikely to be an accreting NS.

By simulating lightcurves that include a periodic signal, we ruled out at the 3σ level periodicities larger than 5.3 s, for a pulsed fraction (e.g., Fürst et al. 2016) of 50%, as well as periodicities larger than 11 s for a pulsed fraction of 30%. The data quality and time resolution do not allow ruling out spin periods smaller than 2 s, like those detected in three NS ULXs (Bachetti et al. 2014; Fürst et al. 2016; Israel et al. 2017b,a), even for a pulsed fraction of 80%. A spin period of 31.6 s, detected in NGC 300 ULX-1 (Carpano et al. 2018), would only go undetected if the pulsed fraction is smaller than 24%, which is smaller than the values found by Carpano et al. (2018). In summary, neither a NS accretor with a $\sim 1 \text{ s}$ spin period, nor a NS with a long spin period but a very low pulsed fraction, can be ruled out for M86 tULX-1. However, a NS with the spin and pulse parameters of NGC 300 ULX-1 can be ruled out confidently.

M86 tULX-1 is among the most variable ULXs of similar or higher luminosity in which the presence of a NS has neither been established nor ruled out (see Sect. 4.1.3). Its variability over a time-scale of at most three years could imply that it is accreting at a sub-Eddington rate (based on the disk instability model, for a review see e.g. Lasota 2001), pointing to a massive BH if that is the case. The relatively hard spectrum compared to other ULXs (e.g., Sutton et al. 2013; Pintore et al. 2017; Walton et al. 2018b) may be an indication of the low/hard state (but this is not necessarily the case), which corresponds to a luminosity of $\lesssim 0.03 L_{\text{Edd}}$ for Galactic BH low-mass X-ray binaries (Maccarone 2003). If that fraction would also apply to M86 tULX-1, then its $L_{\text{Edd}} \gtrsim 2 \times 10^{41} \text{ erg s}^{-1}$, i.e., the Eddington limit of a $\gtrsim 1500 M_\odot$ BH. However, the inner disc temperature depends on the BH mass as $T_{\text{in}} \propto M_{\text{BH}}^{-1/4}$, implying a disc temperature of $\sim 0.1 \text{ keV}$ for accreting BHs that are $\sim 1500 M_\odot$ (Winter, Mushotzky & Reynolds 2006). This is much cooler than the 0.66 keV we fitted for M86 tULX-1 in our combined power-law plus disc blackbody model, which better resembles a stellar-mass BH (Winter et al. 2006).

For these reasons, and because of the rarity of ULXs

this luminous in elliptical galaxies, we consider a relative massive stellar-mass BH of $\sim 30 - 100 M_\odot$ to be a possible accretor in M86 tULX-1. Accretion at or below the Eddington limit would imply a $\gtrsim 48 M_\odot$ BH. A mass of several tens of solar masses is more massive than BHs in Galactic X-ray binaries whose masses have been measured dynamically, but similar to BH masses of around $30 - 60 M_\odot$ observed in the gravitational wave merger event GW150914 (Abbott et al. 2016). Alternatively, M86 ULX-1 could be in the transition region between the normal stellar-mass black holes and the ultraluminous state.

4.3 Companion star

The companion star is likely a giant, as donor stars with low average densities imply long binary orbital periods, and therefore high critical mass transfer rates (e.g., in ‘t Zand et al. 2007; Wu et al. 2010), explaining the unstable accretion disc. Assuming a critical mass transfer rate of $\dot{M}_{\text{crit}} \approx 5 \times 10^{-7} M_\odot \text{ yr}^{-1}$ (based on the peak X-ray luminosity), the orbital period is about 1 – 2 weeks for the range of possibly realistic BH masses of $30 - 1500 M_\odot$ (see Sect. 4.2) (in ‘t Zand et al. 2007, eq. 1). These orbital periods are near the high end of the range seen in Galactic low-mass X-ray binaries (Liu, van Paradijs & van den Heuvel 2007). Any companion stellar type is too faint to be seen by ground-based observations.

4.4 Ruling out alternative explanations

Here we consider explanations for M86 tULX-1 other than a ULX in M86, both extragalactic and Galactic.

4.4.1 Active galactic nucleus

Active galactic nuclei (AGNs) with at least the X-ray flux of M86 tULX-1 occur at a rate of about 3 deg^{-2} (LaMassa et al. 2016), or ~ 0.05 in an area the size of M86. A chance coincidence therefore cannot be ruled out based on X-ray flux alone.

M86 tULX-1 faded to less than 3 per cent of its maximum observed X-ray luminosity within three years. AGNs are not this variable in X-rays over this timespan (e.g., Gibson & Brandt 2012; Lanzuisi et al. 2014; Yang et al. 2016).

The optical data we used and the X-ray data during the bright epoch are not simultaneous, but because AGNs usually vary by less than one magnitude in the optical over several years (e.g., Giveon et al. 1999; Helfand et al. 2001; Kasliwal et al. 2015; Zhang & Feng 2017),² we assumed that M86 tULX-1 had $m_V \gtrsim 23$ during the X-ray bright phase. M86 tULX-1 has a $0.5 - 2 \text{ keV}$ flux of $\sim (1.0 \pm 0.1) \times 10^{-13} \text{ erg s}^{-1} \text{ cm}^{-2}$ using an absorbed POWLAW1D+DISKBB model. Based on LaMassa et al. (2016, their fig. 11), AGNs with fluxes of at least this value have r -band magnitudes brighter than 21, while a few X-ray bright unidentified sources are as faint as $r = 22$. Two AGNs have a $0.5 - 2 \text{ keV}$ flux of $(4 - 5) \times 10^{-14} \text{ erg s}^{-1} \text{ cm}^{-2}$ and $r \approx 23.5 - 25$, which is consistent with M86

² Except for BL Lac objects and related objects, but those are brighter than $m_V = 22$ (Kapanadze 2013) and should have been detected in our deep optical images.

tULX-1 within the error margins, but these two are clear outliers from the sample of ~ 1700 AGNs.

In summary, we conclude that M86 tULX-1 is too optically faint and too strongly variable in X-rays to be an AGN.

4.4.2 Gravitational microlensing event

An object in M86 could cause a microlensing event of an otherwise faint background AGN, leading to a bright X-ray transient. For a range of possible lens masses of $10^{-3} - 1 M_{\odot}$, located in M86, and a source distance assumed to be much larger than the lens distance, we calculated how closely the lens and the source need to be aligned to produce a brightening of a given factor, using equations from Paczyński (1986). The brightening factor must be at least 30 for sources at the detection limit of our 2016 observation, or higher for fainter AGNs. We used the AGN luminosity function by LaMassa et al. (2016, their fig. 3) to calculate the number densities of AGNs available to produce such a brightening, for AGNs up to $3 \times 10^{-15} \text{ erg s}^{-1} \text{ cm}^{-2}$.

The expected number of AGN brightening events in the *Chandra* field of view at any given time is less than 10^{-5} , and unlikely to explain M86 tULX-1. The result is not sensitive to the lens mass or AGN lower limits.

4.4.3 Tidal disruption event

The disappearance of M86 tULX-1 in the 2016 *Chandra* data is consistent with a tidal disruption event (TDE) of a star near a supermassive BH in a galaxy in the background of M86. For a typical X-ray luminosity of $L_X \approx 10^{44} \text{ erg s}^{-1}$ (e.g., van Velzen 2018), the flare of a TDE with the flux of M86 tULX-1 would have a distance of a few Gpc, implying that the host galaxy would have an absolute magnitude fainter than $M_V \approx -18$. Such galaxies are bright enough to host supermassive BHs of order $10^6 M_{\odot}$, typical for TDEs (Auchettl et al. 2017; van Velzen 2018). However, the X-ray spectra of stars disrupted by BHs this massive are typically much softer than observed here (Auchettl et al. 2017). For example, disc blackbody components with temperatures around 50 eV have been measured in the cases of ASASSN-14li (Miller et al. 2015) and ASASSN-15oi (Gezari, Cenko & Arcavi 2017).

4.4.4 Flare star in the Galactic halo

The observed X-ray flux could potentially be caused by coronal X-ray emission from a young Galactic M- or K-dwarf in the foreground of M86, although a decay pattern would be expected over the 148 ks light curve. M86 tULX-1 is located at 15° from the Galactic North Pole, so this star would likely be located in the Galactic halo, rather than the thin or thick discs, unless it has a late M type.

The upper limit for X-ray luminosity L_X relative to bolometric luminosity L_{bol} for coronal flares from a wide range in late-type main sequence stars is usually $L_X/L_{\text{bol}} \lesssim 10^{-2.5}$ (Pizzolato et al. 2003; Wright et al. 2011, and references therein). For the X-ray flux of M86 tULX-1, it follows that the apparent magnitude m_V is brighter than 18, regardless

of its distance. Since the optical brightness of a main sequence star is not expected to vary significantly over several decades, a foreground star close enough to Earth to produce the observed X-ray flux would easily have been detected by the optical survey.

4.4.5 Very faint X-ray transient in the Galactic halo

At a distance of 3 – 30 kpc in the Galactic halo, the flux of M86 tULX-1 corresponds to an X-ray luminosity of $L_X \approx 10^{32-34} \text{ erg s}^{-1}$, which would make it a very faint X-ray binary (VFXRB) (e.g., Degenaar et al. 2012). Given the Galactic latitude of $\sim 75^\circ$, an X-ray binary in the Galactic thin disc would be located within a few 100 pc and be brighter than the observed flux.

Based on the amount of stellar mass in the Galactic halo of $\sim 2 \times 10^9 M_{\odot}$ (e.g., Bullock & Johnston 2005), and the theoretically modelled number of low-mass X-ray binaries of any luminosity per unit stellar mass of $\sim 10^{-7} M_{\odot}^{-1}$ (e.g., Kiel & Hurley 2006; Fragos et al. 2008; van Haaften et al. 2015), about 200 hydrogen-rich X-ray binaries would be expected in the halo. A larger number of hydrogen-poor ultracompact X-ray binaries or their remnants could exist, but for old systems, low average mass transfer rates imply insufficient numbers of observable systems in outburst (van Haaften et al. 2013). This corresponds to $\lesssim 10^{-3}$ in an area on the sky equal to the field of view of a *Chandra* ACIS-I observation (if seen from the Galactic centre; less when seen from Earth), regardless of whether they are bright enough to be detected. However, M86 tULX-1 was not detected in 2016, and in general, many faint X-ray binaries could spend a large fraction of the time below $L_X = 10^{32} \text{ erg s}^{-1}$ (if near 3 kpc) and in particular below $L_X = 10^{34} \text{ erg s}^{-1}$ (if near 30 kpc), placing them below the detection limit of ObsID 15149. Therefore, the detection probability of a Galactic halo X-ray binary in a single *Chandra* observation is a priori significantly lower than 10^{-3} , but cannot be completely ruled out.

4.4.6 Cataclysmic variable

The X-ray flux of M86 tULX-1 is consistent with that of a faint cataclysmic variable (CV) in the Galactic thin disc at a distance of 100 – 300 pc (Worrall et al. 1982), or a brighter CV further out.

No source within 15 arcsec of M86 tULX-1 is detected by the GALEX (Galaxy Evolution Explorer, Martin et al. 2005) All-Sky Imaging Survey in the NUV band (1771 – 2831 Å), with a completeness limit of 22.5 for the area around M86 tULX-1 (Bianchi et al. 2011). These data were taken several years before the M86 tULX-1 bright epoch, but the UV emission from a hot white dwarf is not expected to vary on such a short time-scale.

Non-magnetic CVs are rarely brighter than about $L_X = 10^{32} \text{ erg s}^{-1}$ (Verbunt et al. 1997; Mukai 2017), so non-magnetic CVs beyond a distance of 3 kpc are a very unlikely explanation for M86 tULX-1.

The number of CVs in the halo with the observed flux of M86 tULX-1 per ACIS-I field of view can be estimated by integrating the space density of CVs multiplied by the stellar mass density along the line of sight towards M86 tULX-1. We used the space densities of non-magnetic and magnetic CVs

by Pretorius & Knigge (2012); Pretorius & Mukai (2014) and the stellar mass density by Bullock & Johnston (2005) to calculate a number of less than 10^{-3} per ACIS-I field of view, using conservative assumptions.

4.4.7 Supernova or gamma-ray burst afterglow

A supernova in the elliptical galaxy M86 would be of Type Ia, and those are over 50 times fainter in X-rays than M86 tULX-1 (Russell & Immler 2012). At the distance of M86, such an object should have been detected by optical transient searches.

A gamma-ray burst may have gone undetected, since the full sky is not continuously monitored. However, X-ray afterglows undergo clear decays on day time-scales, even 1 Ms after the burst (Nousek et al. 2006; Liang et al. 2007), and this is not seen in the light curve in Fig. 2.

5 CONCLUSION

The properties of M86 tULX-1 – namely, its high luminosity, location in the field of an elliptical galaxy, relatively hard spectrum, and transient behavior – make this object an unusual ULX. Based on our analysis of both *Chandra* data and ground-based optical imaging, we conclude that it may be a relatively massive stellar-mass black hole accreting from a low-mass giant companion, or a stellar-mass black hole in a transitional state between the normal stellar-mass black holes and those in the ultraluminous state.

Follow-up observations in various bands will potentially be valuable. Of particular use would be an *XMM-Newton* observation during a bright epoch; this would provide a higher-quality spectrum to more accurately determine the object's spectral state (especially if combined with a simultaneous radio observation). Alternatively, obtaining *XMM-Newton* data during a faint epoch would provide more information about the low-hard state. The latter spectrum could be compared to spectra of Galactic X-ray binaries with dynamically measured stellar-mass BH accretors, to estimate the accretor mass in M86 tULX-1. A simultaneous observation by the planned *James Webb Space Telescope* would be able to better constrain the nature of the system, aided by the system's location in a low surface brightness part of M86.

ACKNOWLEDGEMENTS

LMvH thanks Paul H. Sell for discussion of *Chandra* data analysis, Lee Burnside for computer help, and the anonymous referee for valuable suggestions. Support for this work was provided by NASA through Chandra Award Number GO4-15034 issued by the Chandra X-ray Center (CXC), which is operated by the Smithsonian Astrophysical Observatory for and on behalf of NASA under contract NAS8-03060, and by NASA Astrophysics Data Analysis grant NNX15AI71G. The scientific results reported in this article are based on observations made by the *Chandra X-ray Observatory*, and on data obtained from the Chandra Data Archive. This research has made use of software provided by the CXC in the application package CIAO, as well as NASA's Astrophysics Data System Bibliographic Services.

References

- Abbott B. P., et al., 2016, *Phys. Rev. Lett.*, **116**, 061102
- Angelini L., Loewenstein M., Mushotzky R. F., 2001, *ApJ*, **557**, L35
- Arnaud K. A., 1996, in Jacoby G. H., Barnes J., eds, ASPC Vol. 101, Astronomical Data Analysis Software and Systems V. p. 17
- Auchettl K., Guillochon J., Ramirez-Ruiz E., 2017, *ApJ*, **838**, 149
- Bachetti M., 2016, *Astronomische Nachrichten*, **337**, 349
- Bachetti M., et al., 2014, *Nature*, **514**, 202
- Begelman M. C., 2002, *ApJ*, **568**, L97
- Bianchi L., Herald J., Efremova B., Girardi L., Zabot A., Marigo P., Conti A., Shiao B., 2011, *Ap&SS*, **335**, 161
- Brightman M., et al., 2018, *Nature Astronomy*, **2**, 312
- Bullock J. S., Johnston K. V., 2005, *ApJ*, **635**, 931
- Carpano S., Haberl F., Maitra C., Vasilopoulos G., 2018, *MNRAS*, **476**, L45
- Colbert E. J. M., Mushotzky R. F., 1999, *ApJ*, **519**, 89
- Copperwheat C., Cropper M., Soria R., Wu K., 2005, *MNRAS*, **362**, 79
- Copperwheat C., Cropper M., Soria R., Wu K., 2007, *MNRAS*, **376**, 1407
- Dall'Osso S., Perna R., Stella L., 2015, *MNRAS*, **449**, 2144
- Davis S. W., Narayan R., Zhu Y., Barret D., Farrell S. A., Godet O., Servillat M., Webb N. A., 2011, *ApJ*, **734**, 111
- Degenaar N., Wijnands R., Cackett E. M., Homan J., in 't Zand J. J. M., Kuulkers E., Maccarone T. J., van der Klis M., 2012, *A&A*, **545**, A49
- Ekşi K. Y., Andaç İ. C., Çikintoğlu S., Gençali A. A., Güngör C., Öztekin F., 2015, *MNRAS*, **448**, L40
- Fabbiano G., Zezas A., Murray S. S., 2001, *ApJ*, **554**, 1035
- Farrell S. A., Webb N. A., Barret D., Godet O., Rodrigues J. M., 2009, *Nature*, **460**, 73
- Feng H., Kaaret P., 2006, *ApJ*, **653**, 536
- Forbes D. A., Franx M., Illingworth G. D., Carollo C. M., 1996, *ApJ*, **467**, 126
- Fragos T., et al., 2008, *ApJ*, **683**, 346
- Freeman P. E., Kashyap V., Rosner R., Lamb D. Q., 2002, *ApJS*, **138**, 185
- Fürst F., et al., 2016, *ApJ*, **831**, L14
- Gehrels N., 1986, *ApJ*, **303**, 336
- Gezari S., Cenko S. B., Arcavi I., 2017, *ApJ*, **851**, L47
- Gibson R. R., Brandt W. N., 2012, *ApJ*, **746**, 54
- Giveon U., Maoz D., Kaspi S., Netzer H., Smith P. S., 1999, *MNRAS*, **306**, 637
- Gladstone J. C., Roberts T. P., Done C., 2009, *MNRAS*, **397**, 1836
- Heida M., Jonker P. G., Torres M. A. P., 2015, *MNRAS*, **454**, L26
- Helfand D. J., Stone R. P. S., Willman B., White R. L., Becker R. H., Price T., Gregg M. D., McMahon R. G., 2001, *AJ*, **121**, 1872
- in 't Zand J. J. M., Jonker P. G., Markwardt C. B., 2007, *A&A*, **465**, 953
- Irwin J. A., Bregman J. N., Athey A. E., 2004, *ApJ*, **601**, L143
- Irwin J. A., Brink T. G., Bregman J. N., Roberts T. P., 2010, *ApJ*, **712**, L1
- Irwin J. A., et al., 2016, *Nature*, **538**, 356
- Israel G. L., et al., 2017a, *Science*, **355**, 817
- Israel G. L., et al., 2017b, *MNRAS*, **466**, L48
- Joseph T. D., Maccarone T. J., Kraft R. P., Sivakoff G. R., 2015, *MNRAS*, **447**, 1460
- Kaaret P., Feng H., Roberts T. P., 2017, *ARA&A*, **55**, 303
- Kajava J. J. E., Poutanen J., 2009, *MNRAS*, **398**, 1450
- Kapanadze B. Z., 2013, *AJ*, **145**, 31
- Karino S., 2018, *MNRAS*, **474**, 4564
- Kasliwal V. P., Vogeley M. S., Richards G. T., 2015, *MNRAS*, **451**, 4328

- Kaspi V. M., Beloborodov A. M., 2017, *ARA&A*, **55**, 261
- Kiel P. D., Hurley J. R., 2006, *MNRAS*, **369**, 1152
- Kim D.-W., Fabbiano G., 2010, *ApJ*, **721**, 1523
- King A., Lasota J.-P., 2016, *MNRAS*, **458**, L10
- King A. R., Davies M. B., Ward M. J., Fabbiano G., Elvis M., 2001, *ApJ*, **552**, L109
- Koliopanos F., Vasilopoulos G., Godet O., Bachetti M., Webb N. A., Barret D., 2017, *A&A*, **608**, A47
- Kormendy J., Fisher D. B., Cornell M. E., Bender R., 2009, *ApJS*, **182**, 216
- Kosec P., Pinto C., Walton D. J., Fabian A. C., Bachetti M., Brightman M., Fürst F., Grefenstette B. W., 2018, *MNRAS*, **479**, 3978
- LaMassa S. M., et al., 2016, *ApJ*, **817**, 172
- Lanzuisi G., et al., 2014, *ApJ*, **781**, 105
- Lasota J., 2001, *New Astron. Rev.*, **45**, 449
- Liang E.-W., Zhang B.-B., Zhang B., 2007, *ApJ*, **670**, 565
- Lira P., Ward M., Zezas A., Alonso-Herrero A., Ueno S., 2002, *MNRAS*, **330**, 259
- Liu J., 2009, *ApJ*, **704**, 1628
- Liu J., 2011, *ApJS*, **192**, 10
- Liu Q. Z., van Paradijs J., van den Heuvel E. P. J., 2007, *A&A*, **469**, 807
- Maccarone T. J., 2003, *A&A*, **409**, 697
- Maccarone T. J., Kundu A., Zepf S. E., Rhode K. L., 2007, *Nature*, **445**, 183
- Maccarone T. J., Kundu A., Zepf S. E., Rhode K. L., 2010, *MNRAS*, **409**, L84
- Madhusudhan N., Rappaport S., Podsiadlowski P., Nelson L., 2008, *ApJ*, **688**, 1235
- Martin D. C., et al., 2005, *ApJ*, **619**, L1
- Medvedev A. S., Poutanen J., 2013, *MNRAS*, **431**, 2690
- Mei S., et al., 2007, *ApJ*, **655**, 144
- Middleton M. J., Heil L., Pintore F., Walton D. J., Roberts T. P., 2015, *MNRAS*, **447**, 3243
- Miller J. M., et al., 2015, *Nature*, **526**, 542
- Motch C., Pakull M. W., Grisé F., Soria R., 2011, *Astronomische Nachrichten*, **332**, 367
- Motch C., Russell T., Soria R., Grisé F., Pakull M., Miller-Jones J., 2014, *ATel*, **6828**
- Mukai K., 2017, *PASP*, **129**, 062001
- Mushtukov A. A., Suleimanov V. F., Tsygankov S. S., Poutanen J., 2015, *MNRAS*, **454**, 2539
- Nousek J. A., et al., 2006, *ApJ*, **642**, 389
- Ochsenbein F., Bauer P., Marcout J., 2000, *A&AS*, **143**, 23
- Paczyński B., 1986, *ApJ*, **304**, 1
- Patruno A., Zampieri L., 2008, *MNRAS*, **386**, 543
- Peacock M. B., Zepf S. E., 2016, *ApJ*, **818**, 33
- Pinto C., Middleton M. J., Fabian A. C., 2016, *Nature*, **533**, 64
- Pintore F., Zampieri L., Stella L., Wolter A., Mereghetti S., Israel G. L., 2017, *ApJ*, **836**, 113
- Pintore F., et al., 2018, *MNRAS*, **477**, L90
- Pizzolato N., Maggio A., Micela G., Sciortino S., Ventura P., 2003, *A&A*, **397**, 147
- Poutanen J., Lipunova G., Fabrika S., Butkevich A. G., Abolmasov P., 2007, *MNRAS*, **377**, 1187
- Poutanen J., Fabrika S., Valeev A. F., Sholukhova O., Greiner J., 2013, *MNRAS*, **432**, 506
- Pretorius M. L., Knigge C., 2012, *MNRAS*, **419**, 1442
- Pretorius M. L., Mukai K., 2014, *MNRAS*, **442**, 2580
- Rhode K. L., Zepf S. E., 2004, *AJ*, **127**, 302
- Roberts T. P., 2007, *Ap&SS*, **311**, 203
- Russell B. R., Immler S., 2012, *ApJ*, **748**, L29
- Sarazin C. L., Irwin J. A., Bregman J. N., 2000, *ApJ*, **544**, L101
- Shao Y., Li X.-D., 2015, *ApJ*, **802**, 131
- Sivakoff G. R., et al., 2008, *ApJ*, **677**, L27
- Skrutskie M. F., et al., 2006, *AJ*, **131**, 1163
- Soria R., 2007, *Ap&SS*, **311**, 213
- Sutton A. D., Roberts T. P., Middleton M. J., 2013, *MNRAS*, **435**, 1758
- Swartz D. A., Ghosh K. K., Tennant A. F., Wu K., 2004, *ApJS*, **154**, 519
- Swartz D. A., Tennant A. F., Soria R., 2009, *ApJ*, **703**, 159
- Swartz D. A., Soria R., Tennant A. F., Yukita M., 2011, *ApJ*, **741**, 49
- Thompson C., Duncan R. C., 1995, *MNRAS*, **275**, 255
- Tsygankov S. S., Mushtukov A. A., Suleimanov V. F., Poutanen J., 2016, *MNRAS*, **457**, 1101
- Turner T. J., George I. M., Nandra K., Turcan D., 1999, *ApJ*, **524**, 667
- van Haaften L. M., Nelemans G., Voss R., Toonen S., Portegies Zwart S. F., Yungelson L. R., van der Sluys M. V., 2013, *A&A*, **552**, A69
- van Haaften L. M., Nelemans G., Voss R., van der Sluys M. V., Toonen S., 2015, *A&A*, **579**, A33
- van Velzen S., 2018, *ApJ*, **852**, 72
- Verbunt F., Bunk W. H., Ritter H., Pfeffermann E., 1997, *A&A*, **327**, 602
- Walton D. J., et al., 2018a, *MNRAS*, **473**, 4360
- Walton D. J., et al., 2018b, *ApJ*, **856**, 128
- Walton D. J., et al., 2018c, *ApJ*, **857**, L3
- Webb N., et al., 2012, *Science*, **337**, 554
- Winter L. M., Mushotzky R. F., Reynolds C. S., 2006, *ApJ*, **649**, 730
- Worrall D. M., Marshall F. E., Boldt E. A., Swank J. H., 1982, *ApJ*, **255**, 111
- Wright N. J., Drake J. J., Mamajek E. E., Henry G. W., 2011, *ApJ*, **743**, 48
- Wu Y. X., Yu W., Li T. P., Maccarone T. J., Li X. D., 2010, *ApJ*, **718**, 620
- Yang G., et al., 2016, *ApJ*, **831**, 145
- Young M. D., 2016, PhD thesis, Indiana University
- Zampieri L., Roberts T. P., 2009, *MNRAS*, **400**, 677
- Zezas A., Fabbiano G., 2002, *ApJ*, **577**, 726
- Zhang X.-G., Feng L.-L., 2017, *MNRAS*, **464**, 2203

This paper has been typeset from a \LaTeX file prepared by the author.